Letter

Topological characterization of rearrangements in amorphous solids

P. Desmarchelier [1,*] S. Fajardo [1] and M. L. Falk [1,2,3,4]

[1]*Department of Material Sciences and Engineering, Johns Hopkins University, Baltimore, Maryland 21218, USA*
[2]*Department of Mechanical Engineering, Johns Hopkins University, Baltimore, Maryland 21218, USA*
[3]*Department of Physics and Astronomy, Johns Hopkins University, Baltimore, Maryland 21218, USA*
[4]*Hopkins Extreme Materials Institute, Johns Hopkins University, Baltimore, Maryland 21218, USA*

(Received 20 January 2024; accepted 17 April 2024; published 29 May 2024)

In amorphous materials, plasticity is localized and occurs as shear transformations. It was recently shown by Wu *et al.* that these shear transformations can be predicted by applying topological defect concepts developed for liquid crystals to an analysis of vibrational eigenmodes [Z. W. Wu *et al.*, Nat. Commun. **14**, 2955 (2023)]. This study relates the −1 topological defects to the displacement fields expected of an Eshelby inclusion, which are characterized by an orientation and the magnitude of the eigenstrain. A corresponding orientation and magnitude can be defined for each defect using the local displacement field around each defect. These parameters characterize the plastic stress relaxation associated with the local structural rearrangement and can be extracted using the fit to either the global displacement field or the local field. Both methods provide a reasonable estimation of the molecular-dynamics-measured stress drop, confirming the localized nature of the displacements that control both long-range deformation and stress relaxation.

DOI: 10.1103/PhysRevE.109.L053002

It has been long appreciated that structural defects play an essential role in the mechanical behavior of crystalline materials. For instance, their yield stress is determined by the behavior of dislocations [1]. These defects are described as breaks in the invariance of the crystal lattice [2].

In amorphous materials, there is no lattice structure, and it is challenging to define discrete defects linked to deformation. The lack of clearly defined defects inhibits the development of a deformation theory for amorphous materials that is specifically linked to aspects of the atomic structure [3,4]. Consequently, predicting structural features that give rise to a larger-scale deformation remains an area of active investigation [5]. The shear transformations (STs), where the structural relaxation takes place, are characterized by large nonaffine displacements of the atoms [6] and high potential energy release [7]. As such, they are local irreversible atomic displacements that contribute to the transition of the system from one inherent structure to another [8] characteristic of plasticity in glasses. STs can be quantified in terms of number [9,10] and activation energy [11,12]. As such they have been integrated as a fundamental micromechanism into numerous constitutive equations [13–17].

Previous studies have characterized the spatial rearrangement taking place in the STs in two-dimensional (2D) [18–20] and three-dimensional (3D) [21] simulated glasses, and experimentally in colloidal [22] and metallic [23,24] glasses. They are typically analyzed in terms of the nonaffine displacements occurring during a structural relaxation, a review of which has been written by Nicolas and Röttler [25]. In particular, these STs can be described as quadrupolar zones [26]. Moreover, an orientation can be assigned to these quadrupoles [25]. More recently, the concept of topological defect (TD) from the liquid-crystal literature has been applied to the displacement field to characterize STs [27]. Another ongoing and important effort is being made to improve the predictions of the positions of sites susceptible to local rearrangements: the shear transformation zones. Many indicators have been developed, and an overview can be found in the review paper of Richard *et al.* [5]. One of the approaches is to consider the eigenmodes of the system, with features of the lowest-frequency eigenmodes predicting the next instability [28,29]. Very recently, Wu *et al.* also identified TDs within low-frequency eigenmodes to predict the STs [30].

These small-scale STs have long-range repercussions. In particular, the quadrupolar zones give rise to long-range elastic deformations, and these can be described using the Eshelby inclusion model [31]. This has been extensively incorporated into mesoscale models of glass plasticity [18,32,33]. Notably, Albaret *et al.* showed that the stress drop due to relaxation can be accurately estimated using the position and characteristics of the Eshelby inclusions [34]. A similar analysis has been performed to study the orientation [25].

In this Letter, we show that the plastic relaxation can be characterized using the core of the STs and their immediate surroundings. First, the STs are located by characterizing the topological defects within the displacement field, and measuring the orientation and magnitude of each defect. We then show that this information can be used to reproduce the entire displacement field using the Eshelby inclusion model. Finally, we relate the orientation and magnitude of the STs to the stress drops using values estimated from either the global displacement field or from the local displacement around the STs only. The topological character of the STs has yet, to our

*paul.desmarchelier@sorbonne-universite.fr

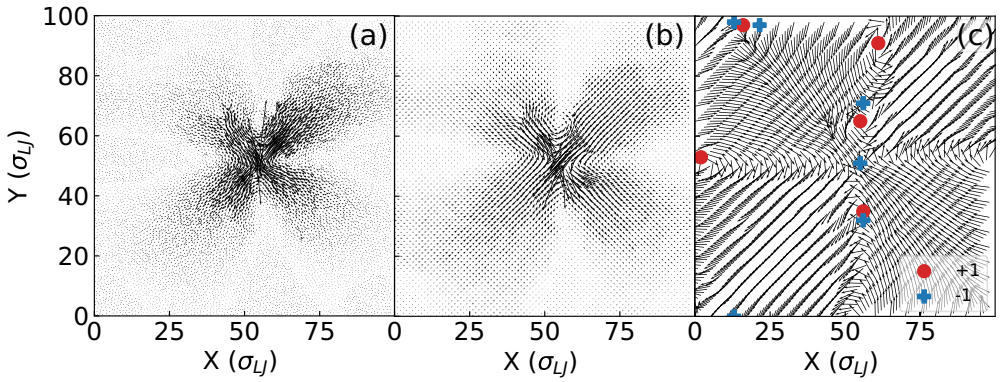

FIG. 1. Representation of the nonaffine displacements during a plastic event: (a) Displacements mapped on atomic positions, (b) coarse-grained displacements, and (c) normed coarse-grained displacement vectors (black arrows) used to determine the topological defect positions (blue crosses for -1 defects and red circles for $+1$ defects).

knowledge, to be linked to their elastic field as described by the Eshelby equations or the magnitude and orientation of the resulting stress relaxation.

The glass samples studied here are 2D binary Lennard-Jones (LJ) glass squares with a side length of 98.8 (Lennard-Jones reduced units) and containing 10 000 atoms, created using the same potential parameters and the slow quench at constant volume approach described by Barbot *et al.* [35]. Fourteen independent samples using different initial spatial distributions are created. These glasses are then deformed in simple shear using an athermal quasistatic (AQS) algorithm [36]. That is, the system is deformed stepwise with a strain step ($\delta\gamma$) of 1×10^{-5} and then relaxed to mechanical equilibrium using a conjugate gradient method before performing the next strain step. This is repeated until a strain (γ) of 0.5 is reached. Lees-Edwards periodic boundary conditions are maintained throughout, and all simulations are performed using LAMMPS [37].

During the deformations, the stress and strain of the whole box are recorded at each deformation step, and the atomic positions are recorded before and after each plastic event. A plastic event, or stress relaxation event, is defined in this study as a shear step that results in the global stresses in the shear direction σ_{xy} decreasing. The impact of this choice is discussed in the Supplemental Material [38]. The nonaffine displacements are computed using the atom positions before the event r_{j-1} and after the event r_j,

$$u_j = r_j - r_{j-1} - u_j^{\text{aff}}, \tag{1}$$

with u_j^{aff} the imposed affine displacement ($u_x = \delta\gamma r_y, u_y = 0$). To represent the nonaffine displacement field corresponding to the structural relaxation, the displacements computed via Eq. (1) are mapped onto the position of the atoms just before the stress drop with the added affine deformation; this is depicted in Fig. 1(a). Additionally, after each stress drop, the stress state after the reversion of a single strain step is computed. The occurrence of a plastic event during this step is very unlikely. This state will be useful for the computation of the shear modulus of the inherent state and is referred to as a reverted state in the following.

The first step of the analysis is to identify the positions of the STs that give rise to the stress drop. This is done by identifying topological defects in the displacement field, in a very similar way to the approach developed by Wu *et al.* [30]. First, atomic displacements are projected onto a 100×100 orthogonal regular grid [see Fig. 1(b)] with the coarse-graining function described by Albaret *et al.* [34] using a length of 1.17 Lennard-Jones distance units (σ_{LJ}). The topological defects are defined by the smallest closed loop for which the topological charge q takes a nonzero value, as defined by the equation [39]

$$\oint d\theta = 2\pi q. \tag{2}$$

Here, θ is the orientation of the displacement [as represented by the orientation of the normed vector in Fig. 1(c)]. As a simplification, the topological defects are computed for each point of the grid by considering a 4×4 square loop around the point considered. Note that the coarse-graining step does not reduce the number of points and is used to ease the implementation of Eq. (2), as suggested by Wu *et al.* [30]. An example of the resulting charges is given in Fig. 1(c). The final position of the defect is the center of mass of the contiguous patches sharing the same topological charge. The quadrupoles and vortices arising upon deformation of a 2D glass [40] will appear as -1 and $+1$ defects, respectively. Importantly, those are the only topological charge values that we observe, meaning that the displacement field can be described as a superposition of quadrupoles and vortices. In Fig. 1(c), a -1 topological charge is detected in the central quadrupolar zone visible in Figs. 1(a) and 1(b), as well as other charges. These other charges appear in regions where the displacements are smaller. Some of these $+1$ charges appear due to the periodic boundary conditions, because the edges of the central quadrupolar zone connect through vortices. Other -1 defects correspond to other minor (characterized by minute displacements) STs. As this analysis stems from nematics, it considers directors and not vectors; as such, the quadrupoles are fourfold symmetric.

More information about the -1 defects can be extracted from the displacement field in their immediate proximity. We assume that the STs are zones that undergo pure shear. This corresponds to the volume-conserving elongation of a circle along a specific orientation. This orientation $\phi_{\text{esh-loc}}$ can be estimated using the angle between the x axis and displacement

of each atom relative to the center of STs. This is done through the phase shift of the second term in the Fourier series of the inner product of the displacement for each atom and their position relative to the center of the ST, i.e.,

$$\phi_{\text{esh-loc}} = \arg\left(\sum_{j=0}^{N_{\text{shell}}} \mathbf{u}_j \cdot (\mathbf{r}_j - \mathbf{x}_{\text{esh}}) \exp(-i2\Omega_j)\right). \quad (3)$$

Here, Ω_j is the angular position of atom j relative to the Eshelby inclusion position ($\mathbf{x}_{\text{esh}}$), and j is the imaginary number. The sum of Eq. (3) runs on all the atoms within 4 interatomic distances of the center of the -1 defect considered (N_{shell}). This approach is similar to the method MD/azi introduced by Nicolas and Röttler [25]. The displacement amplitude near the defects can be used to describe the importance of the defect, both relative to other defects and relative to the global stress relaxation. This can be described using the average atomic nonaffine displacement around the -1 defect that we will denote as $\langle|\mathbf{u}_{\text{na}}|\rangle_{\text{defect}}$. More precisely, we use the contiguous grid positions for which the 4×4 closed loop yield a -1 defect. Their center of mass is shown in Fig. 1(c).

The -1 defects correspond to quadrupoles and can be interpreted as the center of an Eshelby inclusion. The Eshelby inclusion concept assumes that the ST can be modeled as a circular inclusion that has been deformed into an ellipse. Assuming that the medium is homogenous and infinite outside of the inclusion, the following solution, derived by Dasgupta *et al.* [32], can be applied,

$$\begin{aligned} u_x = {} & \frac{\varepsilon^*}{4(1-\nu)}\frac{a^2}{r^2}\left\{\left[2(1-2\nu)+\frac{a^2}{r^2}\right][x\cos 2\phi + y\sin 2\phi]\right. \\ & \left.+\left[1-\frac{a^2}{r^2}\right]\left[\frac{(x^2-y^2)\cos 2\phi + 2xy\sin 2\phi}{r^2}\right]2x\right\}, \\ u_y = {} & \frac{\varepsilon^*}{4(1-\nu)}\frac{a^2}{r^2}\left\{\left[2(1-2\nu)+\frac{a^2}{r^2}\right][x\sin 2\phi - y\cos 2\phi]\right. \\ & \left.+\left[1-\frac{a^2}{r^2}\right]\left[\frac{(x^2-y^2)\cos 2\phi + 2xy\sin 2\phi}{r^2}\right]2y\right\}. \quad (4) \end{aligned}$$

Here, a is the radius of the inclusion; ϕ is the orientation of the quadrupolar zone; r is the distance to the center of the core; x and y describe the position of the center of the inclusion; ε^* is the eigenstrain magnitude; and ν is the Poisson ratio. The Poisson ratio is set at 0.46, based on an AQS tensile deformation simulation of the same glass, and is considered to be homogeneous and constant through the simulation. Equation (4) provides a solution for the displacements outside the core ($r > a$) in an infinite homogeneous medium and can be used to fit the displacement field obtained via molecular dynamics (MD). To this end, the global field is reproduced by summing the displacement fields of all the -1 defects obtained by applying Eq. (4) whenever a stress drop is detected. Thus all the -1 defects are considered, for instance, in Fig. 1(c), including the central negative defect and all the other minor ones. This assumes that the defects are independent. The parameter a is set to $2\sigma_{\text{LJ}}$, and ε^* and ϕ are fitted using a conjugated direction method. As a result, for each event, the displacement field is fitted using two parameters (ε^* and ϕ) per defect. Importantly, only the atoms at a distance greater than $a = 2\sigma_{\text{LJ}}$ away from defects are considered. Details about the fitting process and visualizations of the fitted displacements can be found in the Supplemental Material [38].

The parameters ϕ and ε^* describe the displacements associated with the local ST while $\phi_{\text{esh-loc}}$ and $\langle|\mathbf{u}_{\text{na}}|\rangle_{\text{defect}}$ characterize the displacement field surrounding the ST. Their correlation is displayed in Fig. 2. The link between $\phi_{\text{esh-fit}}$ and $\phi_{\text{esh-loc}}$ appears clearly in Fig. 2(a) with a diagonal distribution showing a one-to-one correspondence. It spans over $[0, \pi/2]$ because of the fourfold symmetry of the quadrupolar zones. The Pearson correlation between the two parameters is 0.26. It also appears that the distribution is not uniform over the whole set of angles, but rather appears centered around $\pi/4$. This $\pi/4$ value corresponds approximately to the orientation of the rearrangement shown in Fig. 1 and aligns with simple shear in the x direction [25,40].

The Eshelby inclusion eigenstrain magnitude ε^* can be characterized by the displacement within the core, and approximated using $\langle|\mathbf{u}_{\text{na}}|\rangle_{\text{defect}}$. As shown in Fig. 2(b), these terms can be linked through a linear fit with a R^2 of 0.72, and this correlation is stable if the fit and correlation are performed on the subset of events for which $\gamma < 0.1$ or $\gamma > 0.3$, or all the events. In this figure, one can also notice that there is an important concentration of ε^* values around 1×10^{-1} and a long tail up to 1×10^{-4}. It can be noted that less than 1%

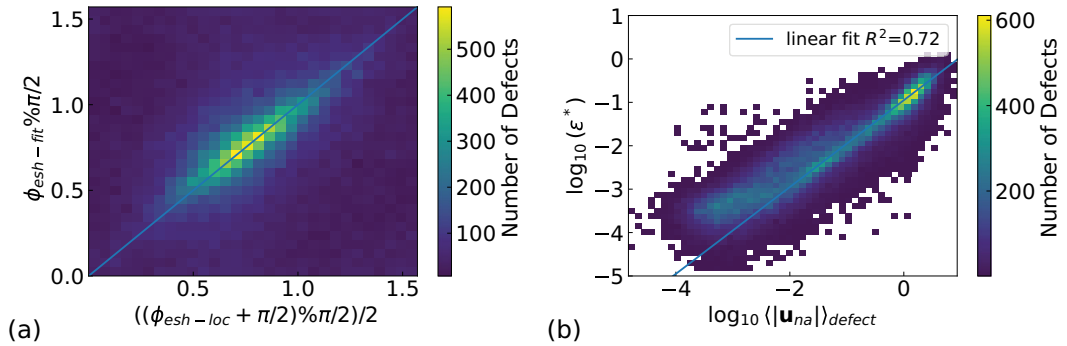

FIG. 2. (a) Distribution of the angle ϕ obtained from the fitting of the whole displacement field to Eq. (4) *vis-à-vis* $\phi_{\text{esh-loc}}$ the angle of the local displacement field from Eq. (3). The diagonal blue line represents one-to-one correspondence. (b) The eigenstrain of the Eshelby equation ε^* *vis-à-vis* the average displacement around the defect. The blue line represents the linear fit.

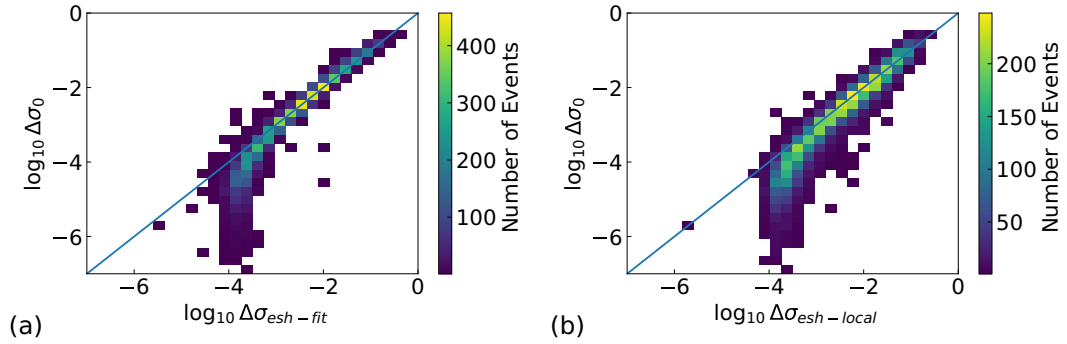

FIG. 3. 2D histogram of the stress drop of each event $\Delta\sigma_0$: (a) as a function of the stress drop computed from Eq. (5) using the parameters obtained with the Eshelby fit $\Delta\sigma_{\text{esh-fit}}$, and (b) compared to using the defect description parameters $\Delta\sigma_{\text{esh-loc}}$. The blue lines representing where the two are exactly equal.

of the defects have an associated ε^* below 1×10^{-10}. These are not displayed in Fig. 2(b). A full distribution of ε^* can be found in the Supplemental Material [38].

As described by Albaret *et al.* [34] the stress drop ($\Delta\sigma_{xy}$) associated with an event can be recomputed by summing the individual contribution of each inclusion,

$$\Delta\sigma_{xy} = \sum^{n_{\text{in}}} \frac{a^2\pi}{V} G_j \varepsilon^* \sin(2\phi), \tag{5}$$

with V the volume of the simulation cell and G_j the shear modulus during event j. This has been obtained by identifying the parameters of Eq. (4) in the equation derived by Albaret *et al.* [34]. From this point on, unless otherwise stated, $\Delta\sigma$ or σ will refer to the xy component, the only one being treated in this study. The shear modulus is estimated using the same method as Albaret *et al.*: It is the difference between the σ_{xy} after the event and on the reverted state divided by $\delta\gamma$. This gives an estimation of the shear modulus of the inherent structure in the absence of plasticity. Other approximations not relying on the reversion of events can be used but do not perform as well for the prediction of $\Delta\sigma$ (see Supplemental Material [38]). As for Eq. (4), a homogeneous medium is assumed. As shown in Fig. 3(a), the MD-derived stress drop $\Delta\sigma_0$ and the value derived from the displacement field fit through Eq. (5), $\Delta\sigma_{\text{esh-fit}}$, have almost a one-to-one correspondence. This is particularly true for stress drops above 1×10^{-3}, which account for most of the stress relaxation [38]. The Pearson correlation coefficient between fitted and MD stress drops is 0.97. More importantly, using the parameters derived from the field displacement in the vicinity of the defects alone yields a similarly good correlation, with the Pearson correlation coefficient shifting to 0.92 as shown in Fig. 3(b). It is also worth mentioning that the distribution of stress drops is not uniform over a range but that there is an important concentration around 1×10^{-2} and a long tail at lower values, much as for the distribution of the eigenstrain magnitudes.

The stress-strain curves can be reproduced by adding the elastic part to the result Eq. (5),

$$\sigma^n_{\text{esh}} = \sum_j^n \Delta\sigma_{\text{esh-}j} + \delta\gamma_j G_j, \tag{6}$$

and are displayed in Fig. 4. Despite the close correspondence observed in Fig. 3(a) the stress is overestimated, meaning that the stress relaxation computed with Eq. (5) is underestimated. This underestimation averages at -3% in relative error, the full distribution can be found in the Supplemental Material [38].

We have shown that the stress drops linked to plastic events are correlated to the displacement field around the -1 topological defects and can be predicted with a fair accuracy across 3 decades.

This analysis is in essence close to the D^2_{min} analysis introduced by Falk and Langer [6] which is still widely used [5], both quantify heterogeneities in the nonaffine displacement

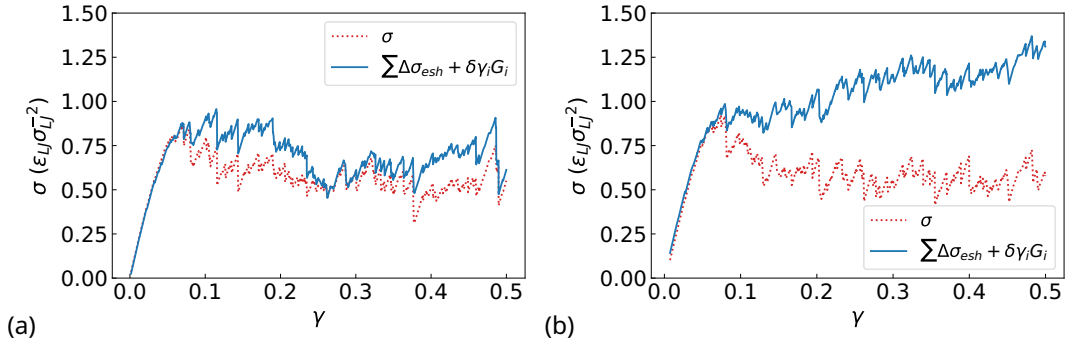

FIG. 4. Stress-strain curves from the simulation (dotted red line), and estimated from Eq. (5) with the parameters fitted from Eq. (4): (a) Example with good correspondence and (b) poor correspondence.

field. But the analysis presented here contains more information and can be used to identify quadrupolar zones (−1 defects) and vortices (+1 defects) [30]. As described by Sopu *et al.* [40], those two structures can be used to describe plastic phenomena in glasses, notably shear banding. Moreover, it is less complex than the method of Fusco *et al.*, which relies on the spatial decay of the plastic energy [7].

Albaret *et al.* previously reproduced the stress-strain curves from the displacement field for a 3D amorphous silicon, with a very good accuracy [34]. This accuracy can partially be attributed to the consideration of a variable inclusion size. We and others have relied on a constant a [32], a ST size that varies from event to event can also be estimated based on the spatial decay of plastic potential energy [34], or the number of atoms having a high D^2_{min} [25]. In those studies, a ranged from 2 to 10 interatomic distances for a-Si and 2 to 20 for the LJ glasses. However, the estimation of the ST size is bound to the estimation of the position of the ST, and this position does not always precisely match the topological defect position. This constant a impacts the value of ε^* leading to an underestimation that explains, at least in part, our inability to consistently reproduce the stress-strain curves as shown in Fig. 4. It might be possible to circumvent this issue by isolating every ST by pinning the atoms of other STs in an auxiliary simulation, as proposed by Nicolas and Röttler [25]. However, this will most probably impact ε^* due to the altered boundary conditions in the immediate surroundings of the inclusion. Moreover, using relative fitting error as defined by Albaret *et al.*, we find a similar distribution. [34]. It is rather spread and provides an estimate with high error for some events, but achieved a lower error for the high-stress drop events (see Supplemental Material [38]).

Due to the elaboration method, the samples are in hydrostatic compression. This will increase the stress at which the deformation appears, as glasses appear to obey a Mohr-Coulomb yield criteria as shown by Lund and Schuh [41]. However, since the deformation is done at a constant volume, this hydrostatic pressure does not induce further relaxation.

This study relies on the formulation of the Eshelby displacement field, which assumes a homogeneous infinite medium. Thus, the solution for individual inclusion does not consider self-interaction through the periodic boundary condition, and a size effect might arise. If there is indeed a size effect observable for smaller sizes, the error seems to stabilize within 3% from a size of $100\sigma_{\text{LJ}}$ on (see Supplemental Material [38]). Moreover, the relative stress drop error distribution is not dependent on the number of events [38]. This hints that the underestimation is not caused by neglecting the interaction between defects, and much less by self-interaction through the boundary conditions. Albaret *et al.* considered the interaction owing to the superposition of displacement fields due to inclusion in periodic images [34], but in our case it does not improve the results and increases the computational cost.

We conclude that there is an essential relationship between the rearrangements that control plasticity and −1 topological defects in the displacement field. They can be used to identify the center of the shear transformations from which quadrupolar relaxation arise. An orientation and magnitude of the eigenstrain can be assigned to these centers either by fitting the displacement field using the Eshelby inclusions model or using the nonaffine displacement in the vicinity of the defect. Using the characteristics of the inclusions obtained from the fits or from the local displacement field, it is possible to obtain a reasonable approximation of the stress relaxation. This reaffirms, with earlier studies [4,8,32,42], that rearrangements in amorphous materials are composed of discrete, local STs that can be enumerated and characterized as such. This is likely true not only in the 3D covalent glasses previously studied by Albaret, but across a wide range of glasses, including metallic glasses and 2D systems. The topological defect concept provides an unambiguous methodology for locating and characterizing such STs.

This work supported by the U.S. National Science Foundation (NSF) under Grant No. DMREF-2323718/2323719/2323720 and was carried out at the Advanced Research Computing at Hopkins (ARCH) core facility [43], which is supported by the NSF under Grant No. OAC 1920103. The authors would like to thank T. Albaret, W. Kob, and T. Curk for fruitful discussion.

[1] V. Vitek, Structure of dislocation cores in metallic materials and its impact on their plastic behaviour, Prog. Mater. Sci. **36**, 1 (1992).

[2] V. Vitek, Atomic level computer modelling of crystal defects with emphasis on dislocations: Past, present and future, Prog. Mater. Sci. **56**, 577 (2011).

[3] M. L. Falk and J. Langer, Deformation and failure of amorphous, solidlike materials, Annu. Rev. Condens. Matter Phys. **2**, 353 (2011).

[4] A. Tanguy, Elasto-plastic behavior of amorphous materials: A brief review, C. R. Phys. **22**, 117 (2021).

[5] D. Richard, M. Ozawa, S. Patinet, E. Stanifer, B. Shang, S. A. Ridout, B. Xu, G. Zhang, P. K. Morse, J.-L. Barrat, L. Berthier, M. L. Falk, P. Guan, A. J. Liu, K. Martens, S. Sastry, D. Vandembroucq, E. Lerner, and M. L. Manning, Predicting plasticity in disordered solids from structural indicators, Phys. Rev. Mater. **4**, 113609 (2020).

[6] M. L. Falk and J. S. Langer, Dynamics of viscoplastic deformation in amorphous solids, Phys. Rev. E **57**, 7192 (1998).

[7] C. Fusco, T. Albaret, and A. Tanguy, Role of local order in the small-scale plasticity of model amorphous materials, Phys. Rev. E **82**, 066116 (2010).

[8] E. Stanifer and M. L. Manning, Avalanche dynamics in sheared athermal particle packings occurs *via* localized bursts predicted by unstable linear response, Soft Matter **18**, 2394 (2022).

[9] F. Delogu, Identification and characterization of potential shear transformation zones in metallic glasses, Phys. Rev. Lett. **100**, 255901 (2008).

[10] J. Yu, A. Datye, Z. Chen, C. Zhou, O. E. Dagdeviren, J. Schroers, and U. D. Schwarz, Atomic-scale homogeneous plastic flow beyond near-theoretical yield stress in a metallic glass, Commun. Mater. **2**, 22 (2021).

[11] B. Xu, M. Falk, J. Li, and L. Kong, Strain-dependent activation energy of shear transformation in metallic glasses, Phys. Rev. B **95**, 144201 (2017).
[12] F. Boioli, T. Albaret, and D. Rodney, Shear transformation distribution and activation in glasses at the atomic scale, Phys. Rev. E **95**, 033005 (2017).
[13] E. Bouchbinder, J. S. Langer, and I. Procaccia, Athermal shear-transformation-zone theory of amorphous plastic deformation. I. Basic principles, Phys. Rev. E **75**, 036107 (2007).
[14] M. L. Manning, J. S. Langer, and J. M. Carlson, Strain localization in a shear transformation zone model for amorphous solids, Phys. Rev. E **76**, 056106 (2007).
[15] C. H. Rycroft, Y. Sui, and E. Bouchbinder, An Eulerian projection method for quasi-static elastoplasticity, J. Comput. Phys. **300**, 136 (2015).
[16] A. R. Hinkle, C. H. Rycroft, M. D. Shields, and M. L. Falk, Coarse graining atomistic simulations of plastically deforming amorphous solids, Phys. Rev. E **95**, 053001 (2017).
[17] K. Kontolati, D. Alix-Williams, N. M. Boffi, M. L. Falk, C. H. Rycroft, and M. D. Shields, Manifold learning for coarse-graining atomistic simulations: Application to amorphous solids, Acta Mater. **215**, 117008 (2021).
[18] A. Tanguy, F. Leonforte, and J. L. Barrat, Plastic response of a 2D Lennard-Jones amorphous solid: Detailed analysis of the local rearrangements at very slow strain rate, Eur. Phys. J. E **20**, 355 (2006).
[19] P. Cao, H. S. Park, and X. Lin, Strain-rate and temperature-driven transition in the shear transformation zone for two-dimensional amorphous solids, Phys. Rev. E **88**, 042404 (2013).
[20] W. Jin, A. Datye, U. D. Schwarz, M. D. Shattuck, and C. S. O'Hern, Using delaunay triangularization to characterize non-affine displacement fields during athermal, quasistatic deformation of amorphous solids, Soft Matter **17**, 8612 (2021).
[21] M. Zink, K. Samwer, W. L. Johnson, and S. G. Mayr, Plastic deformation of metallic glasses: Size of shear transformation zones from molecular dynamics simulations, Phys. Rev. B **73**, 172203 (2006).
[22] P. Schall, D. A. Weitz, and F. Spaepen, Structural rearrangements that govern flow in colloidal glasses, Science **318**, 1895 (2007).
[23] Y. Ma, J. Ye, G. Peng, D. Wen, and T. Zhang, Nanoindentation study of size effect on shear transformation zone size in a Ni–Nb metallic glass, Mater. Sci. Eng., A **627**, 153 (2015).
[24] S. Kang, D. Wang, A. Caron, C. Minnert, K. Durst, C. Kübel, and X. Mu, Direct observation of quadrupolar strain fields forming a shear band in metallic glasses, Adv. Mater. **35**, 2212086 (2023).
[25] A. Nicolas and J. Rottler, Orientation of plastic rearrangements in two-dimensional model glasses under shear, Phys. Rev. E **97**, 063002 (2018).
[26] D. Sopu, A. Stukowski, M. Stoica, and S. Scudino, Atomic-level processes of shear band nucleation in metallic glasses, Phys. Rev. Lett. **119**, 195503 (2017).
[27] M. Baggioli, I. Kriuchevskyi, T. W. Sirk, and A. Zaccone, Plasticity in amorphous solids is mediated by topological defects in the displacement field, Phys. Rev. Lett. **127**, 015501 (2021).
[28] V. Mazzacurati, G. Ruocco, and M. Sampoli, Low-frequency atomic motion in a model glass, Europhys. Lett. **34**, 681 (1996).
[29] A. Tanguy, B. Mantisi, and M. Tsamados, Vibrational modes as a predictor for plasticity in a model glass, Europhys. Lett. **90**, 16004 (2010).
[30] Z. W. Wu, Y. Chen, W.-H. Wang, W. Kob, and L. Xu, Topology of vibrational modes predicts plastic events in glasses, Nat. Commun. **14**, 2955 (2023).
[31] J. D. Eshelby and R. E. Peierls, The determination of the elastic field of an ellipsoidal inclusion, and related problems, Proc. R. Soc. London, Ser. A **241**, 376 (1957).
[32] R. Dasgupta, H. G. E. Hentschel, and I. Procaccia, Yield strain in shear banding amorphous solids, Phys. Rev. E **87**, 022810 (2013).
[33] D. F. Castellanos, S. Roux, and S. Patinet, History dependent plasticity of glass: A mapping between atomistic and elasto-plastic models, Acta Mater. **241**, 118405 (2022).
[34] T. Albaret, A. Tanguy, F. Boioli, and D. Rodney, Mapping between atomistic simulations and Eshelby inclusions in the shear deformation of an amorphous silicon model, Phys. Rev. E **93**, 053002 (2016).
[35] A. Barbot, M. Lerbinger, A. Hernandez-Garcia, R. García-García, M. L. Falk, D. Vandembroucq, and S. Patinet, Local yield stress statistics in model amorphous solids, Phys. Rev. E **97**, 033001 (2018).
[36] C. E. Maloney and A. Lemaître, Amorphous systems in athermal, quasistatic shear, Phys. Rev. E **74**, 016118 (2006).
[37] A. P. Thompson, H. M. Aktulga, R. Berger, D. S. Bolintineanu, W. M. Brown, P. S. Crozier, P. J. in 't Veld, A. Kohlmeyer, S. G. Moore, T. D. Nguyen, R. Shan, M. J. Stevens, J. Tranchida, C. Trott, and S. J. Plimpton, LAMMPS - a flexible simulation tool for particle-based materials modeling at the atomic, meso, and continuum scales, Comput. Phys. Commun. **271**, 108171 (2022).
[38] See Supplemental Material at http://link.aps.org/supplemental/10.1103/PhysRevE.109.L053002 for details on the definition of a relaxation event; the fitting error definition; examples of displacement fields; details of the estimation of the shear modulus; a detailed discussion of the size effect; and a full distribution of ϵ^*.
[39] J. V. Selinger, *Introduction to the Theory of Soft Matter: From Ideal Gases to Liquid Crystals* (Springer, Berlin, 2016).
[40] D. Sopu, STZ-Vortex model: The key to understand STZ percolation and shear banding in metallic glasses, J. Alloys Compd. **960**, 170585 (2023).
[41] A. C. Lund and C. A. Schuh, Yield surface of a simulated metallic glass, Acta Mater. **51**, 5399 (2003).
[42] V. Hieronymus-Schmidt, H. Rösner, G. Wilde, and A. Zaccone, Shear banding in metallic glasses described by alignments of Eshelby quadrupoles, Phys. Rev. B **95**, 134111 (2017).
[43] rockfish.jhu.edu.